



The *IsoStretcher*: An isotropic cell stretch device to study mechanical biosensor pathways in living cells



S Schürmann^a, S Wagner^{a,b}, S Herlitze^a, C Fischer^a, S Gumbrecht^a, A Wirth-Hücking^a, G Pröls^a, LA Lautscham^b, B Fabry^b, WH Goldmann^b, V Nikolova-Krstevski^c, B Martinac^{d,e}, O Friedrich^{a,*}

^a Institute of Medical Biotechnology, Department of Chemical and Biological Engineering, Friedrich-Alexander-University Erlangen-Nürnberg (FAU), Paul-Gordan-Str.3, 91052 Erlangen, Germany

^b Department of Physics, Biophysics Group, FAU, Henkestr. 91, 91052 Erlangen, Germany

^c Molecular Cardiology Division, Victor Chang Cardiac Research Institute, 405 Liverpool St, Darlinghurst, NSW 2010 Sydney, Australia

^d Mechanosensory Biophysics Laboratory, Victor Chang Cardiac Research Institute, Darlinghurst NSW 2010, Australia

^e St Vincent's Clinical School, University of New South Wales, Darlinghurst NSW 2010, Australia

ARTICLE INFO

Article history:

Received 13 October 2015

Received in revised form

7 March 2016

Accepted 8 March 2016

Available online 9 March 2016

Keywords:

Mechanobiology
Cell stretch device
Mechanosensor
Elastomer membrane
Isotropic stretch
Cell stiffness

ABSTRACT

Mechanosensation in many organs (e.g. lungs, heart, gut) is mediated by biosensors (like mechanosensitive ion channels), which convert mechanical stimuli into electrical and/or biochemical signals. To study those pathways, technical devices are needed that apply strain profiles to cells, and ideally allow simultaneous live-cell microscopy analysis. Strain profiles in organs can be complex and multiaxial, e.g. in hollow organs. Most devices in mechanobiology apply longitudinal uniaxial stretch to adhered cells using elastomeric membranes to study mechanical biosensors. Recent approaches in biomedical engineering have employed intelligent systems to apply biaxial or multiaxial stretch to cells. Here, we present an isotropic cell stretch system (*IsoStretcher*) that overcomes some previous limitations. Our system uses a rotational swivel mechanism that translates into a radial displacement of hooks attached to small circular silicone membranes. Isotropicity and focus stability are demonstrated with fluorescent beads, and transmission efficiency of elastomer membrane stretch to cellular area change in HeLa/HEK cells. Applying our system to lamin-A overexpressing fibrosarcoma cells, we found a markedly reduced stretch of cell area, indicative of a stiffer cytoskeleton. We also investigated stretch-activated Ca^{2+} entry into atrial HL-1 myocytes. 10% isotropic stretch induced robust oscillating increases in intracellular Fluo-4 Ca^{2+} fluorescence. Store-operated Ca^{2+} entry was not detected in these cells. The *IsoStretcher* provides a useful versatile tool for mechanobiology.

© 2016 Elsevier B.V. All rights reserved.

1. Introduction

Through mechanotransduction, cells and tissues respond to environmental mechanical stimuli, e.g. pressure, shear stress, deformation. These stimuli connect to external environments but are also vital for sensing the internal milieu to maintain homeostasis, e.g. in the cardiovascular system (Chatterjee and Fisher, 2013; Friedrich et al., 2012). Mechanical stimuli are transformed into intracellular signals, either by direct ion channel modulation (Blumenthal et al., 2014) or via membrane adhesion complex signaling (Janotiak et al., 2013; Martinac, 2014). In hollow organs, cells are exposed to complex strain patterns. Fluctuations in intramural pressure translate to multi-directional or isotropic

cellular stretch (Friedrich et al., 2012), in contrast to more linearly arranged organs, e.g. skeletal muscle (Iwata et al., 2007). However, even muscle cells can differentially sense and respond to various stretch orientations, i.e. uniaxial versus multiaxial (Hornberger et al., 2005). Studying the underlying biosensors requires engineering of complex biomechanics stretch-devices. Many stretch systems operate by linear piezo-driven displacements of thin silicone membranes to which cells are adhered (Yost et al., 2000). A very useful, highly biocompatible, elastomer is PDMS (polydimethylsiloxane). Its viscoelasticity and stiffness can be controlled by appropriate base compound-to-crosslinker ratios (Shi et al., 2013). Substrate stiffness is crucial for cells to tightly adhere and establish focal adhesion connections (Galie et al., 2013). Several uniaxial cell stretch systems have been developed to perform cyclic/static stretch protocols while studying cellular responses using live-cell imaging (Ito et al., 2010; Matsumoto et al., 2007). Most researchers use rectangular PDMS membranes coated

* Corresponding author.

E-mail address: oliver.friedrich@mbt.uni-erlangen.de (O. Friedrich).

with extracellular matrix proteins to which cells are adhered. Membranes are then linearly stretched using attached rods, hooks or clips (Bonakdar et al., 2012; Shao et al., 2013; Yost et al., 2000). Many such systems have shortcomings, e.g. uneven stretch ratios within membrane locations or severe shifts in focal z-length. The latter may limit use in confocal imaging where a large stretch-induced focal plane shift can result in loss of the in-plane image and time-consuming refocussing. Although this can be partially overcome by fine tuning of the PDMS membrane design (Shao et al., 2013), a more physiological mode of cell stretching, involving isotropic or biaxial stretch, has only partly been sufficiently resolved yet. The most popular approach for biaxial stretch involves pneumatic pressure applied to either the PDMS membrane directly (Gavara et al., 2008; Granet et al., 2002), within intermediate Teflon posts (Tan et al., 2008) or stretch by vertical

membrane displacement through an indenter ring (Huang et al., 2010). Majd et al. (2009) introduced an isotropic cell stretcher based on an iris-like diaphragm mechanism involving rotational displacements of eight interdigitating lever arms (Majd et al., 2009) to expand a highly elastic culture dish. This idea prompted us to engineer an advanced isotropic stretch-device that involves rotation of a translation ring containing oblique grooves to which radial hooks were inserted. The continuous rotational movement of the ring is translated into an equal, radial displacement of six hooks clamped to a conically designed circular PDMS membrane. The device performs isotropic stretch in all membrane sectors with acceptable z-shift, which is ideally suitable for high content cell imaging in light or fluorescence microscopy. Our design represents a 'low-cost' solution to study mechanical biosensors in cells compared to commercial systems. We apply this system here

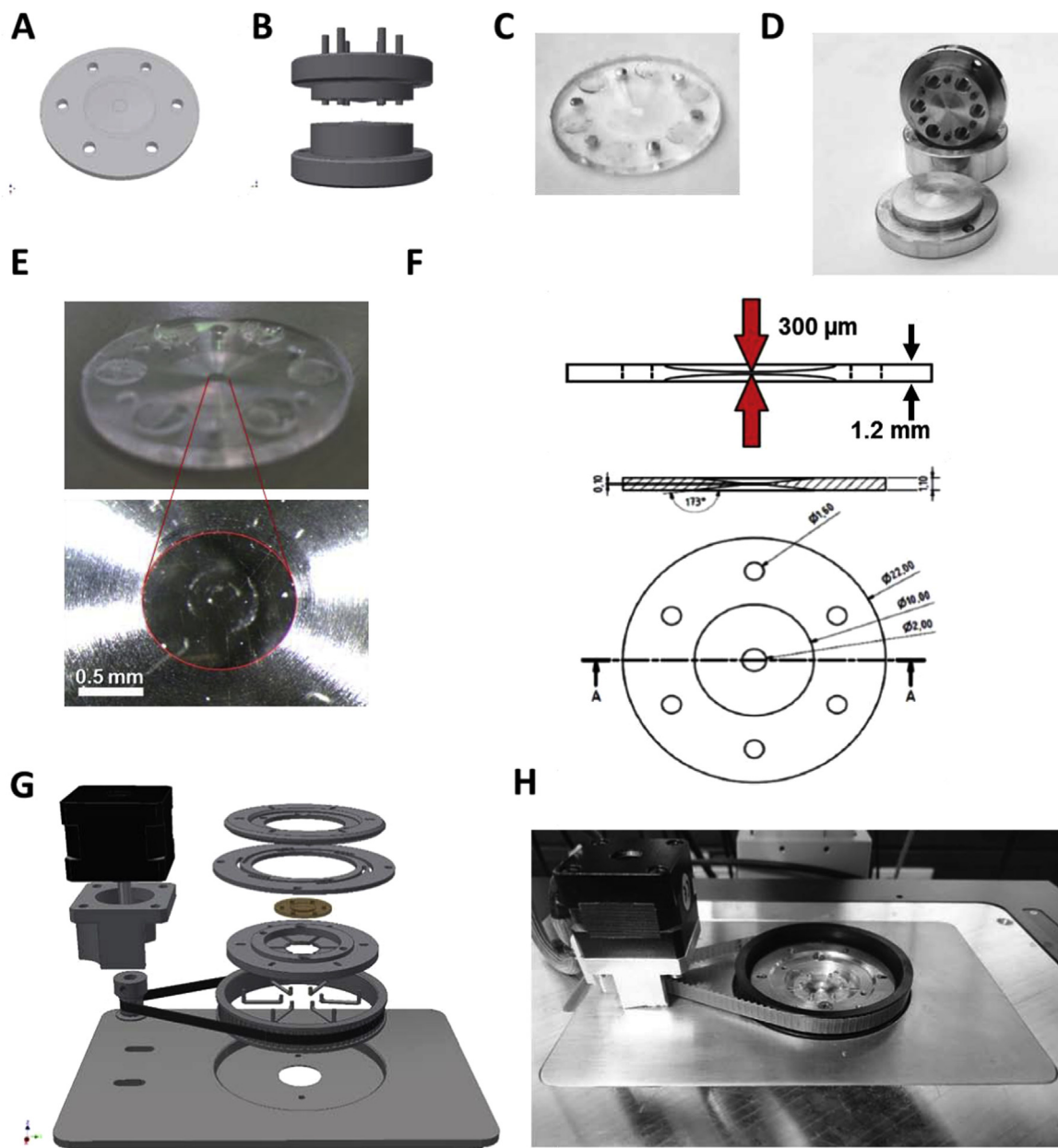


Fig. 1. : Custom-built isotropic cell stretch device (IsoStretcher) and conical design of the PDMS stretch membrane. A,B,F, and G system designs. C,D,E, and H, implementation. A,C, and E, elastic PDMS chamber with a central well for cell substrates and six holes to hold stretcher pins. B, and D, aluminium mold for forming PDMS chambers. E, PDMS membranes after removal from the cast mold and cleaning. Approximate sizes are 1.4 cm in diameter and $\sim 300 \mu\text{m}$ in height at the thinnest center area under slack conditions. F, side view schematics of membrane thickness under slack. G, and H, cell stretcher device. A stepper motor-driven disk with oblique grooves moves six pins along a tangential trajectory and translates their displacement into a radial stretch of the central PDMS chamber.

to study two biologically relevant scenarios: (i) stretch-mediated Ca^{2+} entry into cardiac HL-1 cells and (ii) membrane distensibility in lamin A-overexpressing fibrosarcoma cells.

2. Materials and methods

2.1. Engineering of the IsoStretcher device

Fig. 1 illustrates the design and implementation of our custom-built isotropic stretch device. Central part is an elastic silicone chamber (Fig. 1A, and C) fabricated from polydimethylsiloxane (PDMS) in custom-made aluminium molds (Fig. 1B, and D). It contains a small central reservoir for cell culture and six peripheral holes for mounting the PDMS chambers onto the pins of the *IsoStretcher* (Fig. 1G, and H). The *IsoStretcher* is mounted on an aluminium base-plate that fits on many microscope stages. Six pins are moved radially in linear troughs to apply isotropic stretch to the silicone membrane. Motion of the pins is generated by rotational movement of a disk containing oblique guide grooves. The disk is connected to a stepping motor by a synchronous belt and is driven and controlled by a microcontroller (Arduino Uno R3) and stepper motor board (EasyDriver). A custom-written LabVIEW application based on the LabVIEW-to-Arduino interface (LIFA) was used to control stretch. Full stretch from 0% to 20% requires ~ 1.2 s (~ 0.4 Hz for 20% stretch).

2.2. Design, manufacturing and pre-treatment of PDMS membranes

PDMS membranes were cast using custom-made molds drilled from aluminium blocks as a three-piece cast (Fig. 1B, and D). The top and bottom parts were symmetrically designed to provide a conical shape of decreasing gap distance between the two parts towards the center at a 173° angle (Fig. 1F). Top and bottom parts were placed into a middle ring part containing circular metal spacers that allowed manufacturing of membranes of various thicknesses. The top part contained six evenly spaced pins touching the bottom part when completely assembled. In between, the remaining volume represents the mold volume. We used chambers with a thickness of ~ 1.2 mm at maximum radius and ~ 0.3 mm thickness in the central flat area for cell microscopy. The latter has a diameter of ~ 1.2 mm, roughly matching the field of view of a 10x objective. Reservoir area was around 1 mm^2 . Membranes were cast from dimethylsiloxane (Sylgard 184, Dow Corning) and polymerised by adding a crosslinker (a proprietary platinum-based catalyst, catalysing the addition of the SiH bond across the vinyl groups to form Si-CH₂-CH₂-Si linkages). PDMS is almost incompressible at room temperature, has an approximately linear elasticity with mixture ratios and is highly biocompatible (Carrillo et al., 2005; Lee et al., 2004). A 10:1 ratio of base elastomer and crosslinker, respectively, was mixed and transferred to a vacuum desiccator. The mass was then carefully poured into the casting device, the top part mounted and clamped with a fixture. Venting channels in the upper lid ensured exit of air bubbles and excess elastomer. After polymer curing (60°C for 5 h), the upper lid was removed and the PDMS membrane scraped off the aluminium surface. Protruding polymer pillars (from remaining polymer in vents) were cut off using a surgical blade. Only PDMS membranes that did not show any irregularities within the central area or the hook holes (Fig. 1C, and E) were used with the *IsoStretcher*. The elasticity modulus (E-modulus) of our PDMS membranes was obtained from stress-strain measurements (weights attached to the membranes and measuring length changes). The mean E-modulus was ~ 1.76 MPa, in agreement with published values (Markert et al., 2013). To validate stretch trajectories of surface points on the PDMS membranes within the *IsoStretcher*, $2.5 \mu\text{m}$ fluorescent beads (ThermoFisher Scientifics, Germany) were coated on the PDMS

membranes by evaporation of a bead-ethanol suspension. Images of beads were taken at different stretches and trajectories analysed using a custom-written MatLab program.

To adhere cells to the PDMS membranes, the PDMS hydrophobic surface was pre-treated ('etched') to increase hydrophilicity for cell attachment. Etching was achieved by immersing the central PDMS membrane area in a 1:1 mixture of H_2O_2 and 1 M HCl for 2 h at 37°C . After washes with sterile water, PDMS membranes were coated with extracellular matrix proteins. In order to validate the *IsoStretcher*, we performed experiments on selected cell lines available: HeLa cells, HEK (human embryonic kidney) cells, HT1080 fibrosarcoma cells and atrial myocyte HL-1 cells. For HL-1 cells, PDMS coating consisted of gelatine-fibronectin mixtures (200:10 $\mu\text{g}/\text{ml}$, overnight, 37°C). For HeLa, HEK and HT1080 cells, coating involved 10 mM PEG-silane (2 h, 37°C) followed by PBS washes and laminin coating (20 $\mu\text{g}/\text{ml}$, 1 h). Cell suspension was added to coated PDMS membranes and cell adhesion allowed overnight.

2.3. Cell culture and imaging procedure of HeLa, HEK, HT1080 *LamA*⁺ and HL-1 cells on PDMS membranes

Details of cell seeding and imaging are given in the [Supplementary material](#).

2.4. Image and statistical analysis

Images of cell borders (bright-field) and Ca^{2+} -fluorescence intensity were analysed in manually assigned ROIs using ImageJ software by a student blinded to the stretch conditions. This approach may arguably be more subjective, yet produced more robust results as compared to several anticipated automated analysis approaches in ImageJ or MatLab, since in particular in bright-field images, the low contrast of unstained cells precluded a reliable segmentation of cell borders (note: HEK cell data involving fluorescent membrane staining could be analysed using automated segmentation by thresholding). Moreover, from the calibration of fluorescent bead z-focus with stretch (Fig. 2), a mean tabulated z-shift with stretch was implemented into a macro to correct the z-position of the objective for each stretch position prior to acquiring a new image. For bright-field images, the remaining uncertainty of z-focus with stretch was counteracted by recording a small z-stack of images, quickly driving the objective z-position from $-15 \mu\text{m}$ to $+15 \mu\text{m}$ of the projected z-focus rather than taking one single image. From the stack images that were recorded, the best-focused image was chosen for analysis. The aforementioned corrections were not available for the confocal microscope. Data are given as box plots (median, quartiles and 1–99% whiskers) or as mean \pm SEM with number of observations (n).

3. Results

3.1. Isotropic stretch and small z-shifts of PDMS membranes in the IsoStretcher

To validate the isotropicity of stretch, trajectories of fluorescent beads were tracked. Fig. 2A confirms an equal stretch in all directions with the *IsoStretcher*. Single beads move on radial traces with small central displacements and larger peripheral movements. More important than the overall movement of single beads is an assessment of their relative distances during stretch. An example of the distance between four individual beads forming a trapezoid is shown in Fig. 2B. The area of the trapezoid clearly increases with applied stretch. Fig. 2C shows box plots of the measured stretch distances in x and y direction as a function of the

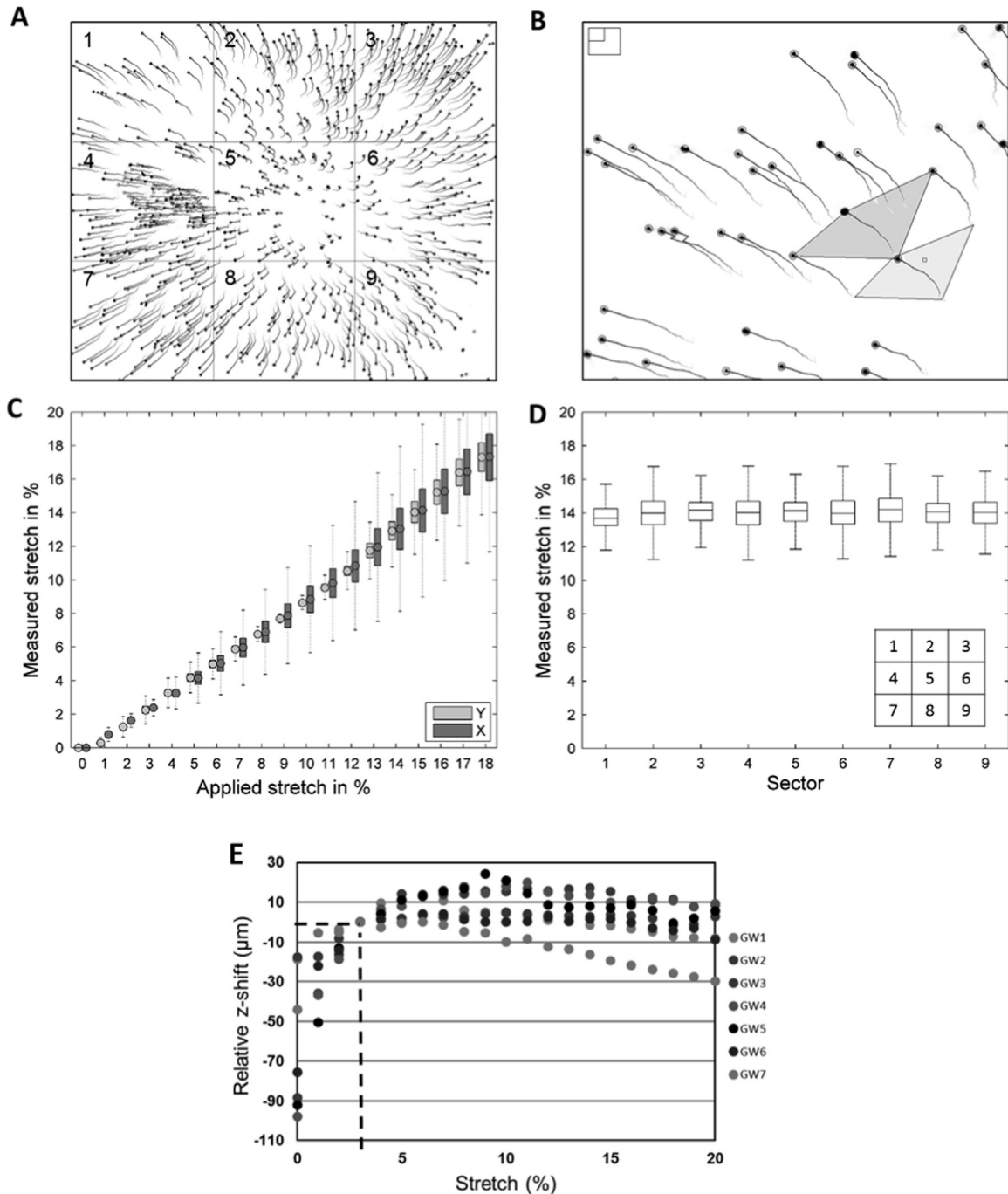


Fig. 2. : Isotropic stretch of PDMS membranes and z-focus shift quantification during stretch. A, fluorescent beads tracked during 0–18% isotropic stretch. Traces illustrate radial displacements. B, magnified view of sector 1. The distance between neighboring particles increases upon stretch, illustrated by two connecting polygons at 0% and 18% stretch. C, stretch along x- and y-direction measured between all neighboring particles for all beads. Measured stretch shows linear dependence on applied stretch with no significant difference between x- and y-component. D, measured stretch along y-direction at 15% applied stretch, for each of the nine sectors, shows uniform behavior within the entire field-of-view. E, analysis of z-focus shifts during isotropic stretch in PDMS membranes made from seven casting devices (GW1–GW7). Z-focus shift normalized to the z-value at 3% stretch. C and D, show box plots with the median value as horizontal line, the upper and lower quartiles and the whiskers marking the 1–99% percentiles.

applied stretch between hundreds of neighboring particles on the membrane. The results show a good translation of stretch to the PDMS membrane. The measured stretch of all beads was analysed in nine membrane sectors and confirmed uniformity of the applied stretch to the whole PDMS membrane for a representative stretch to 15% (Fig. 2D). To validate the suitability of our stretch system for live-cell imaging, we analysed the extent of z-plane shift during increasing stretch in PDMS membranes produced from our seven equally engineered casting devices. As during the initial 2–3% of stretch, z-shift scatters were large due to different slack conditions

among individual membranes, the actual slack tension was assumed at a stretch of 3%, to which all subsequent z-values were normalized. Between 2% and 20% of applied stretch, the focal shift of the membrane was only $\sim 10 \mu\text{m}$, on average (Fig. 2E). Such a small drift can be well compensated either on systems running an automated focus correction or by manual focus adjustment between stretches. In our case, we implemented a macro to drive the objective z-position to a new z-value deposited in a mean z-shift-stretch matrix obtained from Fig. 2E.

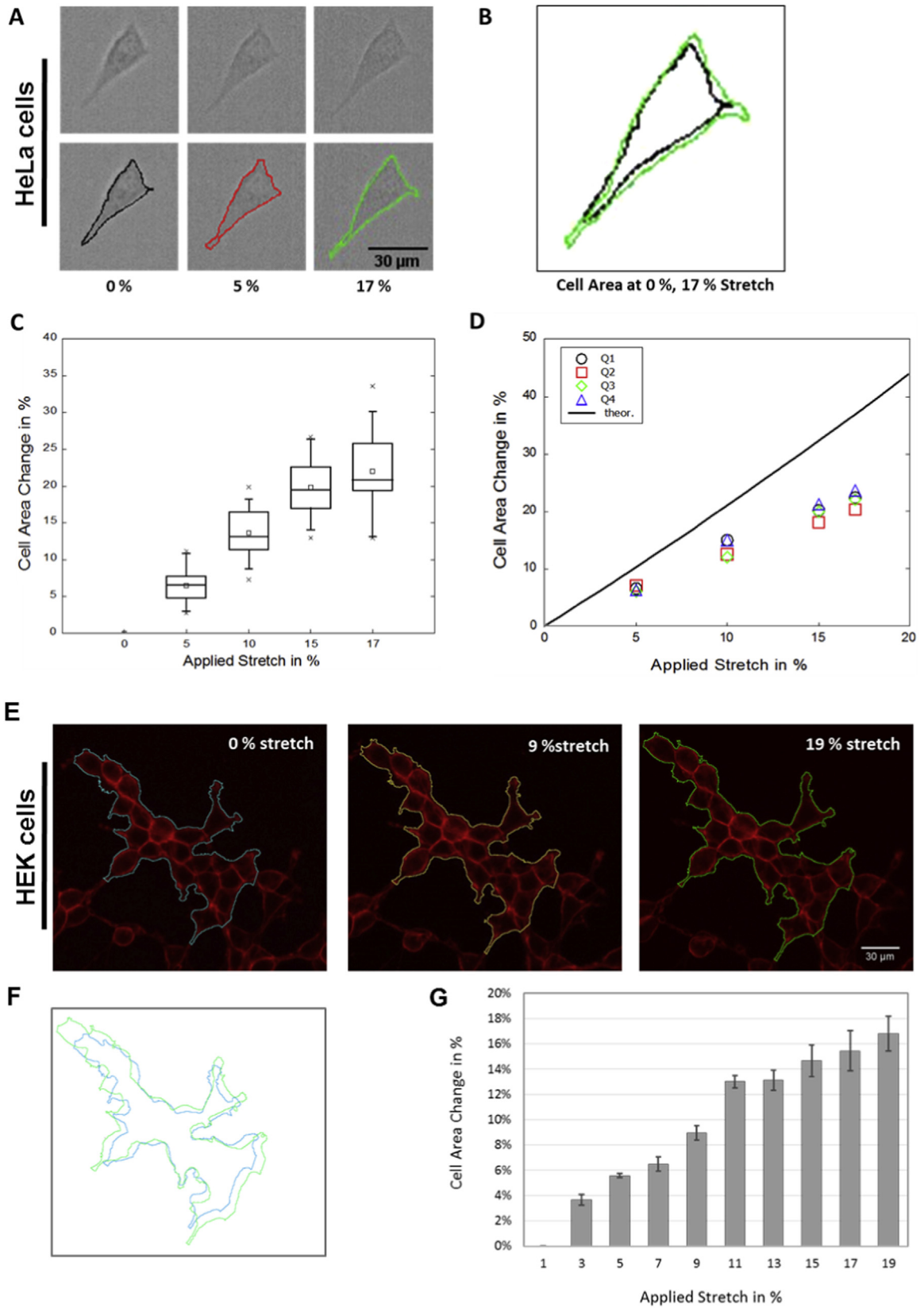


Fig. 3. : Stretch of HeLa cells. A, single HeLa cell at 0, 5% and 17% applied stretch. Cell borders were traced manually. B, overlay of the cell border traces at 0% and 17% stretch clearly shows an increase in cell area. C, relative cell area measured for 16 cells at different stretch levels. D, mean values of measured cell area change evaluated separately in four quadrants. Solid line represents the theoretical area increase for the applied stretch. E, fluorescence images of live HEK cells, stained with Evans Blue to highlight the cell membrane, at 0%, 9% and 19% of applied stretch. Cell borders were traced automatically with a threshold based method in ImageJ. F, overlay of the cell ensemble border traces at 0% and 19% stretch shows the increase in cell area. G, relative area of HEK cells at different stretch levels (average based on three different thresholding methods).

3.2. Translation of PDMS membrane stretch to adherent HeLa and HEK cells

The results so far confirm a good translation of ‘hardware-set’ stretch (calculated from the degree of swivel motor rotation to radial pin displacement) to the 2D plane stretch of the PDMS membrane. However, this does not yet correspond to the effective stretch to the cell membrane area since the translated stretch depends on the tightness of cell adherence to the ECM-coated PDMS membrane. In principle, this has to be evaluated for each cell type separately. As an example for epithelial cells, the human epithelial carcinoma cell line HeLa was used to validate the stretch transmission from PDMS to cellular membrane. Fig. 3A, and B show images of a single adherent HeLa cell subjected to various stretches in the *IsoStretcher* as indicated. A clear increase in cellular circumference can be detected. This is evaluated for the relative cell area change in 16 HeLa cells for a range of stretch levels in Fig. 3C for the whole membranes and separated by four quadrants (Fig. 3D). It is interesting to note that the measured increase in surface area falls behind the theoretical increase, assuming a 1:1 translation of mechanical stretch, which already indicates that this strongly depends on the tightness of the cell-matrix junction. Also, the deficit becomes larger for larger stretches > 10%, which is indicative of partial disruptions of the cell-matrix fixation, i.e. focal adhesions. For up to 10% stretch, it can be stated that stretch applied to the PDMS membrane is well transmitted to HeLa cells growing on this substrate resulting in an increase in projected cell area. The importance of this calibration of applied PDMS stretch to actual membrane area stretch translation is further documented by the responses of HEK cells coated to our PDMS membranes and stained for membrane fluorescence (Fig. 3 E–G, suppl. movie 1). The cells nicely follow the overall membrane stretch (suppl. movie), the detailed membrane area analysis shows a similar behavior for the HeLa cells with an approximate 16% cell area change upon the largest stretches.

Supplementary material related to this article can be found online at <http://dx.doi.org/10.1016/j.bios.2016.03.015>.

3.3. Cell membranes are stiffer in HT1080 cells overexpressing lamin-A

The above results suggest that stretch regimes up to 10% are well transduced to cell membranes, at least in epithelial-like cells embedded in Matrigel. We next wanted to elucidate the effects of the nuclear lamina protein lamin-A on cell membrane mechanics during

isotropic stretch. Nuclear lamina is a filamentous meshwork comprised of lamin proteins that line the inner nuclear membrane and provide structural support to the nucleus and attachment sites for nuclear and cytoskeletal proteins (Lammerding et al., 2006). Lamin-A overexpressing (~threefold) HT1080 fibrosarcoma cells (LamA⁺), also expressing a GFP-tag at the lamin A N-terminus, were subjected to 5–15% isotropic stretch and compared with controls.

Fig. 4A shows a representative example of GFP-signals originating from the nuclei of Lamin-A⁺ cells under slack and 10% stretch. Statistical analysis showed reduced increase in cell area in the Lamin-A⁺ cells compared with controls up to 10% stretch, indicative of a stiffer cell membrane. This is in line with recent findings where cell stiffness was about two times increased in LamA⁺ cells (Lautscham et al., 2015). For 15% stretch, all Lamin-A⁺ cells detached from the PDMS membrane, while this accounted only for a few of the control cells. Also, in the aforementioned study (Lautscham et al., 2015), adhesiveness of Lamin-A⁺ HT1080 cells was about one third reduced compared to controls.

3.4. Demonstration of stretch-activated, but not store-operated Ca²⁺ entry in cardiac HL-1 cells

Apart from a recently demonstrated shear-stress induced mechanosensitivity of Na⁺ current depolarisation in HL-1 cells (Strege et al., 2012), nothing is known about mechanosensitive Ca²⁺ entry in HL-1 cells, in contrast to adult cardiomyocytes (Friedrich et al., 2012). Therefore, stretch-activated Ca²⁺ entry was analysed in HL-1 cells. Fig. 5A shows images from HL-1 cells isotropically stretched to 10% in Ca²⁺-free medium. First, thapsigargin was added to deplete intracellular Ca²⁺ stores, reflected by the first Ca²⁺ release peaks in stretched HL-1 cells (note: individual cells may respond with variable time delay to thapsigargin, as indicated in four individual cell responses in the right panel thus, broadening the thapsigargin response in the averaged group presentation). Then, Ca²⁺ was re-introduced to the bathing solution, which led to a robust induction of Ca²⁺ oscillations and sustained increase in intracellular Ca²⁺. To rule out or quantify any contribution from store-operated Ca²⁺ entry (SOCE), the same protocol was repeated in unstretched HL-1 cells adhered to the PDMS membrane. As shown in Fig. 5B, the cells responded to thapsigargin by a transient increase in Fluo-4 fluorescence. However, introduction of Ca²⁺ to the external bath did not result in any further increase in Fluo-4 fluorescence, which is indicative of no contribution of SOCE in stretched HL-1 cells.

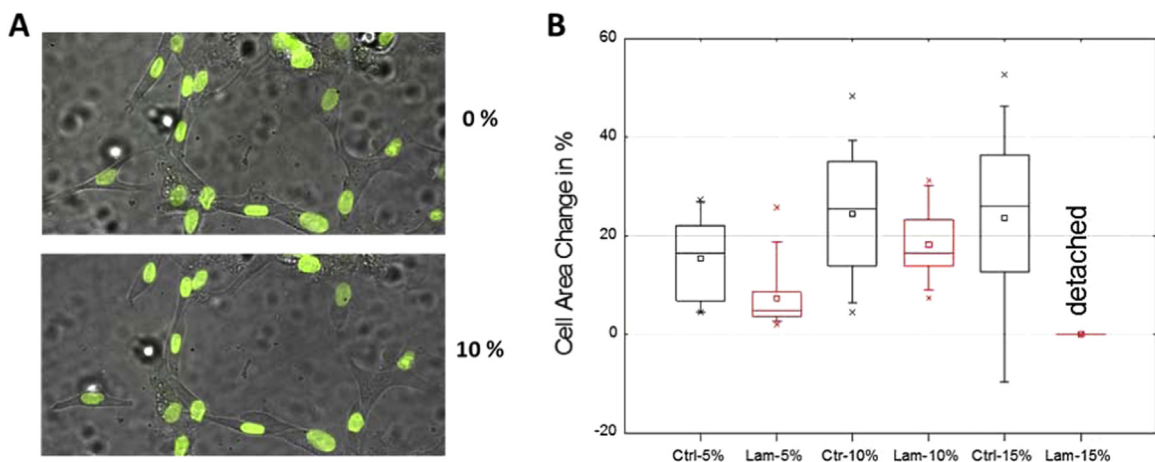
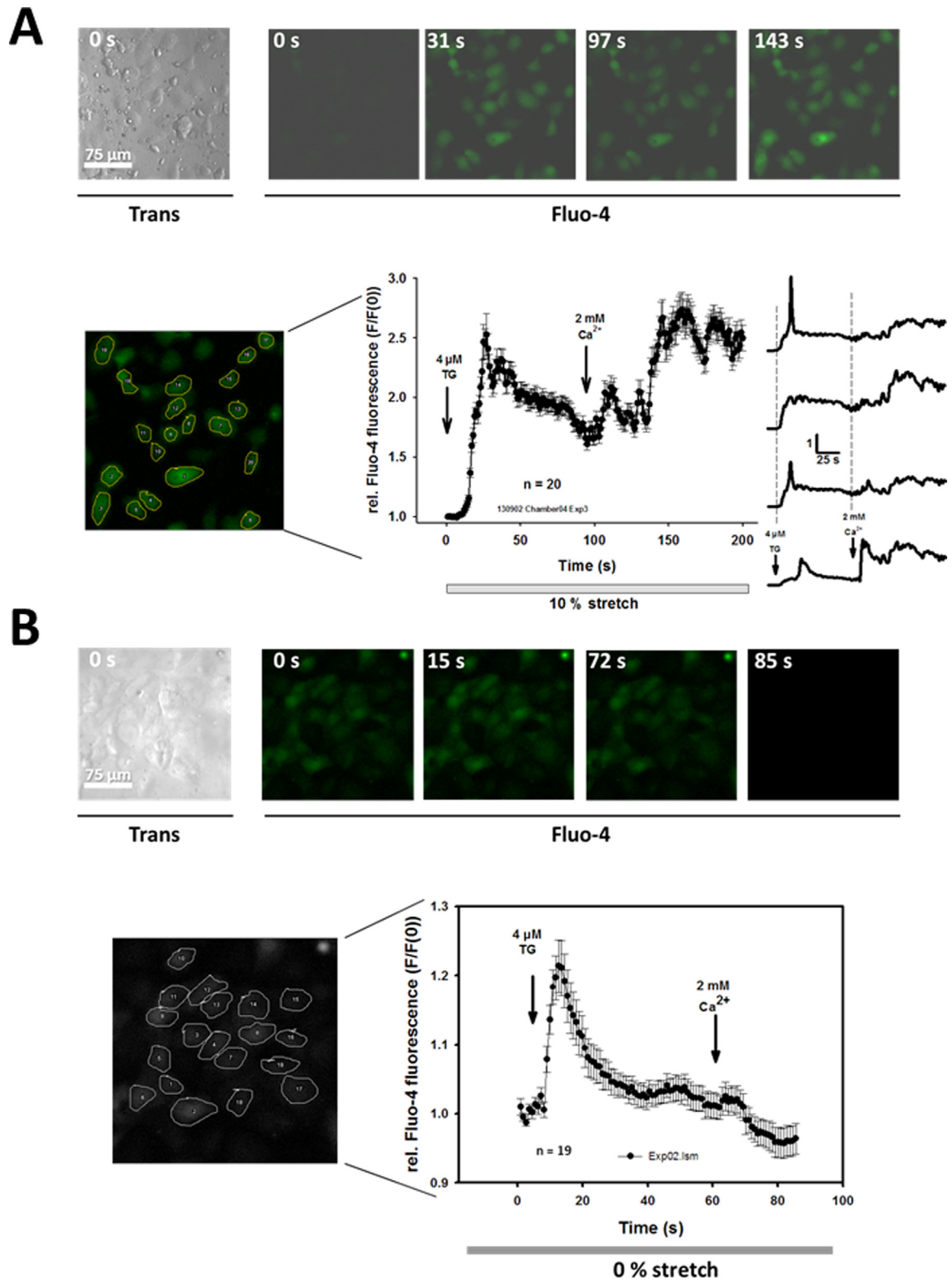


Fig. 4. : Isotropic stretch of Lamin-A overexpressing HT1080 cells. A, image of HT1080 cells (Lamin-A overexpressing, GFP-tag) at 0% and 10% applied stretch. B, cell area change observed at 5%, 10% and 15% applied stretch is lower in Lamin-A overexpressing cells (red boxes) compared to control cells (black boxes). At 15% stretch, all Lamin-A overexpressing cells completely (not further evaluated) and few control cells partially detached from the PDMS membrane resulting in low relative cell area changes. (For interpretation of the references to color in this figure legend, the reader is referred to the web version of this article.)



4. Discussion

4.1. Advantages of the IsoStretcher over other conventional systems

We chose a mechanical actuator-driven approach implementing a rotational swivel motor to drive an intermediate transmission ring with oblique grooves, where metal hooks were embedded in a linear trough to be radially displaced as the ring was turned. This system has the advantage of a transmission of rotation angle to radial displacement of the hooks clamping a circular PDMS membrane. The isotropicity of stretch was confirmed tracing fluorescent beads. Relative stretch was equally distributed over the PDMS membrane. The design of the conically-shaped thin PDMS membranes allowed for a reduced focal z-shift of (on average) 10 μm at 10% stretch, the smallest so far reported. This represents an improvement over pneumatic systems (Kreutzer et al., 2014). Since all parts are off-the-shelf mechanical/electrical components implemented on the Arduino board, the pure material costs of our system are in the range of 200 USD, including the cast devices. Several previous biaxial/multi-axial systems relied on pneumatically induced stretch of an elastomer membrane, either by suction to the membrane directly or to interdigitating post pillars. Although the first approach nicely simulates complex multi-axial cyclic strains, such as found in distending hollow organs, the membrane bending during pneumatic extension introduces substantial curvature and displacement, which renders it unsuitable or at least difficult for live-cell imaging. Under such conditions, cells were usually fixed and stained for microscopy following the mechanical strain protocols. For example, Tan et al. (2008) subjected rat vascular smooth muscle cells to cyclic multi-axial strain applying -20 kPa vacuum sinusoidal pressure fluctuations for 24 h. Their membranes were designed with micro-groove patterns to generate anisotropic biaxial micro-gradients. In post-stretch fixed cells, strain anisotropy only had minor effects on F-actin expression (Tan et al., 2008). In order to overcome the constraints imposed by a direct vertical extension of the base-membrane through pneumatic suction on microscopy, pioneering work by AJ Banes introduced loading posts underneath the elastomeric membrane. By applying suction, the membrane is sucked into the corridor set between the loading posts and the chamber walls, effectively resulting in a planar stretch of cells, either uniaxially or biaxially, depending on post geometry (Banes, 2013; Dhein et al., 2014; Garvin et al., 2003). Although this technology has been commercialized by FlexCell[®] Int., a major provider for mechanobiology research (Banes, 2013), its main application has been on imaging of fixed cells following prolonged cyclic stretch protocols (e.g. Dhein et al., 2014; Garvin et al., 2003; Wang et al., 2015) rather than live-cell imaging (De Jonge et al., 2013). One reason might be potentially large focus shifts during stretch that may render such systems prone to elaborate refocussing during live cell imaging involving confocal microscopy, to a much larger extent than tolerable, for instance, during epifluorescence or white light transmission imaging (Ahearne et al., 2008). Interestingly, the focal z-shifts in FlexCell[®] systems seem not well documented in the literature. Also, in the FlexCell[®] systems, lubricants required to enhance membrane sliding over posts were described to disturb visualization of cells, and the large loading posts themselves completely block visualization of cells on inverted microscopes (Kreutzer et al., 2014). In order to overcome those constraints, Kreutzer et al. (2014) developed a pneumatically actuated, post-free, biaxial stretch system consisting of a thin PDMS membrane, an outer and inner PDMS shell and a rigid glass plate. By applying vacuum pressure to the cavity between shells, the elastic PDMS membrane was deformed thus, buckling the inner shell symmetrically into radial direction (Kreutzer et al., 2014). This system proved suitable for use with inverted microscopes however, their

calibration of in-plane-strain with vacuum pressure and out-of-focus displacement documented a marked focus shift during stretch, e.g. 300–350 μm at 10% strain. Wang et al. (2010) also used a pneumatically-driven approach with a vacuum chamber within a thick PDMS layer (support walls) connected to a thin PDMS membrane of 50 μm thickness that slides over a glass cover-slip upon suction. This way, focal membrane shifts could be minimised through adhesive forces by introducing a silicone oil between PDMS membrane and cover slip, while the latter allowed for high NA immersion inverted microscopy. However, focal shifts were not quantified (Wang et al., 2010). It should be noted that Rapalo et al. recently published a very similar approach to ours, presenting an in-plane mechanical stretch device utilizing six evenly spaced clamps attached to the flexible membrane allowing a maximum linear strain of 20% (Rapalo et al., 2015). Membrane strain was linearly translated to adherent human bronchial epithelial cells as judged from linear distance measurements of DAPI stained nuclei under a confocal microscope pre- and post-stretch (Rapalo et al., 2015). However, the actual increase in cell membrane area by applying equiaxial stretch was not assessed. This is important since the actual confirmation of cell membrane area increase is a crucial determinant of the transmission efficiency of PDMS membrane stretch to the cell membrane and depends on the tightness of mechanical linkage.

4.2. Coating conditions and cell adherence to the PDMS membrane

Living cells do not adhere directly to PDMS membranes and require special coatings. The mechanical linkage to extracellular matrix coatings (laminin, fibronectin, collagen, etc.) is determined by local cytoskeletal architecture and the amount and distribution of focal adhesions (FAs). The latter was shown to crucially depend on the substrate stiffness in adult cardiomyocytes cultured on PDMS membranes. When the extracellular environment was too stiff or too soft, cells began to remodel (Galie et al., 2013). Cell borders and FA protein distributions under uniaxial and biaxial stretch conditions were monitored in bovine aortic endothelial cells using an indenter-ring-based stretch of an elastomeric membrane; a modular indenter design allowed switching between equiaxial and uniaxial strain profiles (Huang et al., 2010). The authors confirmed cell border transmission of elastomeric membrane stretch to compute the extent of cellular deformation at 14% stretch. Cell membrane area stretch closely matched the expected magnitude of substrate stretch, and cells created more FAs when subjected to biaxial stretch compared to uniaxial stretch (Huang et al., 2010). In our system, the increase in cell area was also confirmed up to 15% stretch. Higher stretches resulted in membrane areas below the expected theoretical increase, most probably because of focal adhesions disruption and mechanical uncoupling of cells from the substrate. Thus, it is important to assess optimum coating conditions and maximum mechanical transmission confidence for each cell type.

4.3. Mechanical cell-substrate coupling and stiffness in lamin-A overexpressing cells

Lamin-A determines nuclear shape and mechanics (Lammerding et al., 2006) and connects between the nuclear interior and the cytoskeleton (Lombardi et al., 2011). While lamin A/C deficiency promotes defects in nuclear structure, mechanics (i.e. increased nuclear deformation, decreased cytoskeletal stiffness) and dilative cardiomyopathy (Lammerding et al., 2004; Nikolova et al., 2004), effects of lamin-A overexpression are less known. In melanoma cells overexpressing recombinant lamin A, reduced nuclear deformability was found (Ribeiro et al., 2014). Lamin A overexpression in HT1080 cells was recently shown to be associated

with decreased cell adhesiveness and increased stiffness (Lautscham et al., 2015). Since no literature data are available on cellular mechanics under isotropic stretch in cells with stiffened nuclear envelopes, we isotropically stretched Lamin-A⁺ HT1080 cells. The stiffening of the nucleus also transmits to a stiffening of the cytoskeleton and the membrane area, as evidenced by a reduced increase in cell area compared to control cells for stretches up to 10% (an alternative explanation is a partial detachment from within the 3D Matrigel matrix). At 15% stretch, the increased stiffness of the mutant HT1080 cells resulted in a complete detachment of cells within the Matrigel hydrogel. These results confirm the stiffening of the global cellular cytoskeleton through isolated increase in nuclear stiffness in Lamin-A⁺ cells.

4.4. Mechanosensitive Ca²⁺ entry in isotropically stretched cardiac HL-1 cells

The importance of external mechanical load on mechano-chemical transduction and Ca²⁺ signaling in adult cardiomyocytes was recently demonstrated using a *cell-in-gel* system in gel-embedded cardiomyocytes (Jian et al., 2014). Although no stretch was applied then, it already showed that cardiomyocytes require a complex 3D matrix environment for adequate assessment of FAs. Preliminary results with our *IsoStretcher* system confirmed that 2D coating to PDMS was not successful to obtain a firm adherence of adult cardiomyocytes for isotropic stretch. While 3D embedding in hydrogels is ongoing work in our lab, we turned to cardiac HL-1 cells that show adult phenotypic characteristics (Claycomb et al., 1998) and good adherence to coated PDMS membranes. Ca²⁺ homeostasis has been studied in conjunction with disease models, e.g. atrial fibrillation (Xiao et al., 2010) or RyR2 mutations (Jiang et al., 2005), but never under stretch conditions. Our results from HL-1 cells stretched to 10% with the *IsoStretcher* clearly show a marked stretch-induced Ca²⁺ entry that was absent under control conditions. Since we emptied intracellular Ca²⁺ stores, the Ca²⁺ dynamics observed could be a superposition of store-operated (SOCE) and mechano-activated Ca²⁺ entry. However, the former was excluded since under control conditions, no SOCE was detected. This is an interesting finding suggesting non-existence of SOCE in atrial HL-1 cells, which has not been addressed before. In adult ventricular cardiomyocytes, SOCE was documented over the last years (Kojima et al., 2012; Völkers et al., 2010) and recently, also in human atrial myocytes (Zhang et al., 2013). This may point towards an important difference in fully differentiated atrial cardiomyocytes versus murine immortalised HL-1 cells unravelled by our *IsoStretcher* approach.

5. Conclusion and outlook

We designed a cell stretch system that is suitable for live-cell imaging of cells under conditions of defined mechanical stretch to study mechanical biosensors in living cells and their mechano-sensitive signaling pathways. Our system provides isotropic stretch of cells adhered to a PDMS membrane up to ~15% with acceptable shifts in optical focus plane. The system is compact, adaptable to many microscopes and has the advantages of low cost and increased throughput compared to systems using uniaxial stretch in isolated single cells (Prosser et al., 2011). With this system, we gained new insights into cellular stiffening by lamin-A overexpression and stretch-activated Ca²⁺ entry in HL-1 cells. Potential future applications of this system are clearly in the field of mechanobiology and mechano-bioengineering to study and identify cellular mechano-biosensors in cells and their effect to cell biology and tissues.

Acknowledgements

Partly funded by the German Academic Exchange Service (DAAD, #57058305, #57214153 to OF, WHG), Group-of-eight (Go8) (to BM), Deutsche Forschungsgemeinschaft (to BF FA367-2) and the Australian National Health and Medical Research Council (NHMRC, # APP1108013 to OF, VNK, BM).

Appendix A. Supporting information

Supplementary data associated with this article can be found in the online version at <http://dx.doi.org/10.1016/j.bios.2016.03.015>.

References

- Ahearne, M., Bagnaninchi, P.O., Yang, Y., Haj, A.J.E., 2008. *J. Tissue Eng. Regen. Med.* 2, 521–524.
- Banes, A.J., 2013. *Ann. Biomed. Eng.* 41 (9), 1926–1938.
- Blumenthal, N.R., Hermanson, O., Heinrich, B., Shastri, V.P., 2014. *Proc. Natl. Acad. Sci. USA* 111 (45), 16124–16129.
- Bonakdar, N., Luczak, J., Lautscham, L., Czonstke, M., Koch, T.M., Mainka, A., Jungbauer, T., Goldmann, W.H., Schröder, R., Fabry, B., 2012. *Biochem. Biophys. Res. Commun.* 419 (4), 703–707.
- Carrillo, F., Gupta, S., Balooch, M., Marshall, S.J., Marshall, G.W., Pruitt, L., Puttlitz, C. M., 2005. *J. Mater. Res.* 20 (10), 2820–2830.
- Chatterjee, S., Fisher, A.B., 2013. *Antioxid. Redox Signal.* 20 (6), 899–913.
- Claycomb, W.C., Lanson, Jr.N.A., Stallworth, B.S., Egeland, D.B., Delcarpio, J.B., Bahinski, A., Izzi, Jr.N.J., 1998. *Proc. Natl. Acad. Sci. USA* 95 (6), 2979–2984.
- De Jonge, N., Baaijens, F.P., Bouten, C.V., 2013. *J. Vis. Exp.* 80, e51009.
- Dhein, S., Schreiber, A., Steinbach, S., Apel, D., Salameh, A., Schlegel, F., Kostelka, M., Dohmen, P.M., Mohr, F.W., 2014. *Prog. Biophys. Mol. Biol.* 115 (2–3), 93–102.
- Friedrich, O., Wagner, S., Battle, A.R., Schürmann, S., Martinac, B., 2012. *Prog. Biophys. Mol. Biol.* 110 (2–3), 226–238.
- Gavara, N., Roca-Cusachs, P., Sunyer, R., Farre, R., Navajas, D., 2008. *Biophys. J.* 95 (1), 464–471.
- Galie, P.A., Khalid, N., Carnahan, K.E., Westfall, M.V., Stegemann, J.P., 2013. *Cardiovasc. Pathol.* 22 (3), 219–227.
- Garvin, J., Qi, J., Maloney, M., Banes, A.J., 2003. *Tissue Eng.* 9 (5), 967–979.
- Granet, C., Vico, A.G., Alexandre, C., Lafage-Proust, M.H., 2002. *Cell Signal.* 14 (9), 679–688.
- Hornberger, T.A., Armstrong, D.D., Koh, T.J., Burkholder, T.J., Esser, K.A., 2005. *Am. J. Physiol. Cell. Physiol.* 288, C185–C194.
- Huang, L., Mathieu, P.S., Helmke, B.P., 2010. *Ann. Biomed. Eng.* 38 (5), 1728–1740.
- Ito, S., Suki, B., Numaguchi, Y., Ishii, M., Iwaki, M., Kondo, M., Naruse, K., Hasegawa, Y., Sokabe, M., 2010. *Am. J. Respir. Cell. Mol. Biol.* 43 (1), 26–34.
- Iwata, M., Hayakawa, K., Murakami, T., Naruse, K., Kawakami, K., Inoue-Miyazu, M., Yuge, L., Suzuki, S., 2007. *Pathobiology* 74 (3), 159–168.
- Janotiak, R., Brabek, J., Auernheimer, V., Tatarova, Z., Lautscham, L.A., Dey, T., Gemperle, J., Merkel, R., Goldmann, W.H., Fabry, B., Rösel, D., 2013. *Cell. Mol. Life Sci.* 71 (4), 727–744.
- Jian, Z., Han, H., Zhang, T., Puglisi, J., Izu, L.T., Shaw, J.A., Onofriok, E., Erickson, J.R., Chen, Y.J., Horvath, B., Shimkunas, R., Xiao, W., Li, Y., Pan, T., Chan, J., Banyasz, T., Tardiff, J.C., Chiamvimonvat, N., Bers, D., Lam, K.S., Chen-Izu, Y., 2014. *Sci. Signal.* 7 (317), ra27.
- Jiang, D., Wang, R., Xiao, B., Kong, H., Hunt, D.J., Choi, P., Zhang, L., Chen, S.R., 2005. *Circ. Res.* 97 (11), 1173–1181.
- Kojima, A., Kitagawa, H., Omatsu-Kanbe, M., Matsuura, H., Nosaka, S., 2012. *Br. J. Anaesth.* 109 (3), 352–360.
- Kreutzer, J., Ikonen, L., Hirvonen, J., Pekkanen-Mattila, M., Aalto-Setälä, K., Kallio, P., 2014. *Med. Eng. Phys.* 36, 396–501.
- Lammerding, J., Fong, L.G., Ji, J.Y., Reue, K., Stewart, C.L., Young, S.G., Lee, R.T., 2006. *J. Biol. Chem.* 281 (35), 25768–25780.
- Lammerding, J., Schulze, P.C., Takahashi, T., Kozlov, S., Sullivan, T., Kamm, R.D., Stewart, C.L., Lee, R.T., 2004. *J. Clin. Invest.* 113 (3), 370–378.
- Lautscham, L.A., Kämmerer, C., Lange, J.R., Kolb, T., Mark, C., Schilling, A., Strissel, P. L., Strick, R., Gluth, C., Rowat, A.C., Metzner, C., Fabry, B., 2015. *Biophys. J.* 109 (5), 900–913.
- Lee, J.N., Jiang, X., Ryan, D., Whitesides, G.M., 2004. *Langmuir* 20, 11684–11691.
- Lombardi, M.L., Jaalouk, D.E., Shanahan, C.M., Burke, B., Roux, K.J., Lammerding, J., 2011. *J. Biol. Chem.* 286, 26743–26753.
- Majd, H., Wipff, P.J., Buscemi, L., Bueno, M., Vonwil, D., Quinn, T.M., Hinz, B., 2009. *Stem Cells* 27, 200–209.
- Markert, C.D., Guo, X., Skardal, A., Wang, Z., Bharadwaj, S., Zhang, Y., Bonin, K., Guthold, M., 2013. *J. Mech. Behav. Biomed. Mater.* 27, 115–127.
- Martinac, B., 2014. *Biochim. Biophys. Acta* 1838, 682–691.
- Matsumoto, T., Yung, Y.C., Fischbach, C., Kong, H.J., Nakaoka, R., Mooney, D.J., 2007. *Tissue Eng.* 13 (1), 207–217.
- Nikolova, V., Leimena, C., McMahon, A.C., Tan, J.C., Chandar, S., Jogia, D., Kesteven, S.

- H., Michalíček, J., Otway, R., Verheyen, F., Rainer, S., Stewart, C.L., Martin, D., Feneley, M.P., Fatkin, D., 2004. *J. Clin. Invest.* 113 (3), 357–369.
- Prosser, B.L., Ward, C.W., Lederer, J.W., 2011. *Science* 333, 1440–1445.
- Rapalo, G., Herwig, J.D., Hewitt, R., Wilhelm, K.R., Waters, C.M., Roan, E., 2015. *J. Vis. Exp.* 102, e52737.
- Ribeiro, A.J., Khanna, P., Sukumar, A., Dong, C., Dahl, K.N., 2014. *Cell. Mol. Bioeng.* 7 (4), 544–551.
- Shao, Y., Tan, X., Novitski, R., Mugaddam, M., List, P., Williamson, L., Fu, J., Liu, A.P., 2013. *Rev. Sci. Instrum.* 84 (11), 114304.
- Shi, Y., Dong, Y., Duan, Y., Jiang, X., Chen, C., Deng, L., 2013. *Mol. Med. Rep.* 7 (2), 419–424.
- Strege, P., Beyder, A., Bernard, C., Crespo-Diaz, R., Behfar, A., Terzic, A., Ackermann, M., Farugia, G., 2012. *Channels* 6 (6), 457–462.
- Tan, W., Scott, D., Belchenko, D., Qui, H.J., Xiao, L., 2008. *Biomed. Micro.* 10 (6), 869–882.
- Völkers, M., Salz, M., Herzog, N., Frank, D., Dolatabadi, N., Frey, N., Gude, N., Friedrich, O., Koch, W.J., Katus, H.A., Sussman, M.A., Most, P., 2010. *J. Mol. Cell. Cardiol.* 48 (6), 1329–1334.
- Wang, D., Xie, Y., Yuan, B., Xu, J., Gong, P., Jiang, X., 2010. *Integr. Biol.* 2, 288–293.
- Wang, Y., Xiong, Z., Gong, W., Zhou, P., Xie, Q., Zhou, Z., Lu, G., 2015. *Exp. Cell Res.* 338 (1), 39–44.
- Xiao, J., Liang, D., Zhao, H., Liu, Y., Zhang, H., Lu, X., Liu, Y., Li, J., Peng, L., Chen, Y.H., 2010. *Exp. Biol. Med.* 235, 862–868.
- Yost, M.J., Simpson, D., Wrona, K., Ridley, S., Ploehn, H.J., Borg, T.K., Terracio, L., 2000. *Am. J. Physiol. Heart Circ. Physiol.* 279, H3124–H3130.
- Zhang, Y.H., Wu, H.J., Che, H., Sun, H.Y., Cheng, L.C., Li, X., Au, W.K., Tse, H.F., Li, G.R., 2013. *Pflug. Arch.* 465 (10), 1439–1449.